Magnetic quenching of the inverse cascade in rapidly rotating convective turbulence

Stefano Maffei, Michael A. Calkins, Keith Julien, and Philippe Marti

Phys. Rev. Fluids **4**, 041801 — Published 8 April 2019

DOI: 10.1103/PhysRevFluids.4.041801

Magnetic quenching of the inverse cascade in rapidly rotating convective turbulence

Stefano Maffei,[1] Michael A. Calkins,[1] Keith Julien,[2] and Philippe D. Marti[3,4]

[1]*Department of Physics, University of Colorado, Boulder, Colorado 80309, USA*

[2]*Department of Applied Mathematics, University of Colorado, Boulder, Colorado 80309, USA*

[3]*Center for Climate System Modeling, ETH Zürich, CH-8092, Switzerland*

[4]*Department of Earth Sciences, ETH Zürich, CH-8092, Switzerland*

(Dated: March 7, 2019)

Abstract

We present results from an asymptotic magnetohydrodynamic model that is suited for studying the rapidly rotating, low viscosity regime typical of the electrically conducting fluid interiors of planets and stars. We show that the presence of sufficiently strong magnetic fields prevents the formation of large-scale vortices and saturates the inverse cascade at a finite length-scale. This saturation corresponds to an equilibrated state in which the energetics of the depth-averaged flows are characterized by a balance of convective power input and ohmic dissipation. A quantitative criteria delineating the transition between finite-size flows and domain-filling (large-scale) vortices in electrically conducting fluids is found. By making use of the inferred and observed properties of planetary interiors, our results suggest that convection-driven large-scale vortices do not form in the electrically conducting regions of many bodies.

The subsurface regions of stars and the fluid cores of planets are typically characterized by rapid rotation, buoyancy-driven convective turbulence, and electromagnetic fields generated by the dynamo mechanism that converts the kinetic energy of fluid motion into electromagnetic energy. The dynamical state of such systems is characterized by several non-dimensional parameters, including the Reynolds number, $Re_H = UH/\nu$, the Ekman number, $E_H = \nu/(2\Omega H^2)$, and the Rossby number, $Ro_H = U/(2\Omega H)$. Here U and H represent a typical speed and length-scale of the flow, ν is the kinematic viscosity and Ω is the rotation rate. The Reynolds, Ekman and Rossby numbers represent the relative sizes of inertia to viscous forces, viscous forces to the Coriolis force, and inertia to the Coriolis force, respectively. Rapidly rotating turbulent flows are characterized by $Re_H \gg 1$ and $E_H \ll Ro_H \ll 1$. An important physical property of electrically conducting fluids is the magnetic Prandtl number, $Pm = \nu/\eta$, where η is the magnetic diffusivity. For the Earth's liquid outer core these parameters are estimated to be $Re_H \approx 10^8$, $E_H \approx 10^{-15}$, $Ro_H \approx 10^{-7}$ and $Pm \approx 10^{-6}$ [1]. In contrast, the most extreme direct numerical simulation (DNS) spherical dynamo study to date [2] used values of $E_H = 5 \times 10^{-8}$ and $Pm = 10^{-1}$, and reached $Re_H \approx 5 \times 10^3$. Although of crucial importance for understanding magnetohydrodynamics (MHD), it is unknown how the results of such DNS studies extrapolate to natural systems. For flows with sufficiently large values of Re_H, and subject to a broad variety of forcing mechanisms, rapidly rotating three-dimensional turbulence gives rise to the formation of motions with large lateral scales relative to the forcing scale [3–7]. Such flows result from an inverse energy cascade that leads to a net transfer of kinetic energy from the small-scale motions to large-scale motions of the flow. For hydrodynamic, non-magnetic turbulence, the ultimate scale at which the inverse cascade ceases is dependent upon the geometry. In a Cartesian geometry with equal horizontal dimensions, the cascade leads to domain-filling large-scale vortices (LSVs) [5, 7, 8]. In a spherical geometry, the inverse cascade is halted at the so-called Rhines scale [9]. The Rhines scale represents a dynamical cross-over between eddy dynamics that dominate on small-scales and Rossby wave dynamics that dominate on large-scales; it is thought to control the latitudinal extent of alternating winds in the outer, electrically-insulating fluid regions of giant planet atmospheres [10].

It has been suggested, based on the results of DNS studies [8, 11, 12], that inverse-cascade-generated LSVs might be important for generating large-scale (i.e. domain-scale) magnetic fields in planets and stars. However, rapid rotation alone is sufficient for generating large-

scale magnetic fields [13], even for laminar, small-Reynolds-number flows that lack an inverse cascade [14–16]. In the asymptotic limit of rapid rotation, LSVs are unimportant for the onset of dynamo action [16]. However, the influence of magnetic field on the inverse cascade remains poorly understood due, in large part, to the limited parameter range of previous DNS studies. It is evident that the Rossby number, in particular, is not low enough in many DNS investigations to be applicable to planetary systems; this effect is evident in DNS studies in which LSVs shows a preference for cyclonic circulation (i.e. in the same direction as the system rotation vector) [4, 8]. For sufficiently small Rossby numbers the LSV consists of a dipolar vortex with no preference for a particular circulation direction [17]. Thus, lower Rossby number simulations are necessary to better understand the planetary regime.

It should be noted that rapid rotation is not a requirement for the inverse cascade. Previous work has shown that imposed magnetic fields can also lead to an inverse energy cascade [18–20]. In addition, studies of two-dimensional turbulence have shown that sufficiently strong magnetic fields [21] and Lorentz-force-like forcing terms [22] can disrupt the inverse cascade. Here we find that a similar effect occurs in rapidly rotating, convection-driven turbulence, which represents a system that is more applicable to the study of planets and stars.

Although previous work has suggested that the presence of magnetic fields can prevent the formation of large-scale structures in rapidly rotating convective systems [12], no systematic study has been performed to date that fully elucidates the physical mechanism by which a magnetic field influences the inverse cascade. In this regard, we explore the problem by utilizing an asymptotically reduced form of the governing equations of MHD [13], that is valid in the geo- and astrophysically relevant limits of $(E_H, Ro_H, Pm) \to 0$ with $Re_H \gg 1$. We consider rotating Rayleigh-Bénard convection in a horizontally-periodic plane layer of incompressible fluid of depth H, with constant vertical gravity and rotation vectors ($\mathbf{g} = -g\mathbf{e}_z$ and $\mathbf{\Omega} = \Omega\mathbf{e}_z$, respectively, where $\mathbf{e}_z$ is the vertical unit vector). A constant temperature difference $\Delta\theta$ between the top and bottom boundaries is maintained to drive convective motions. Here we provide only a brief overview of the derivation of the model. Further details can be found in previous work [13, 15, 16, 23, 24]. We assume that the small convective spatial scale l and the Rayleigh number $Ra_H = g\alpha\Delta\theta H^3/(\kappa\nu)$ (α is the thermal expansion coefficient and κ is the thermal diffusivity) scale, respectively, as $E_H^{1/3}H$ and $E_H^{-4/3}$, as informed from linear theory [25]. These scalings ensure scale separation between l

and the depth of the layer such that $\epsilon \equiv l/H = E_H^{1/3} \ll 1$, which translates into separation between the small-scale coordinate system (x, y, z) and the domain-scale, vertical coordinate $Z = \epsilon z$. The equations are separated into mean (averaged over the small horizontal scales) and fluctuating components. We then expand each dependent variable (f, say) in a power series of the form $f = f_0 + \epsilon^{1/2} f_{1/2} + \epsilon f_1 + \ldots$, take the limit $\epsilon \to 0$, and collect terms of equal magnitude in the resulting system of equations. Upon integrating on the small vertical coordinate z, we obtain the following system for the asymptotically reduced equations (where the ordering subscripts on the variables have been dropped):

$$D_t^\perp \zeta - \partial_Z w = \widetilde{Q}\, \overline{\mathbf{B}} \cdot \nabla_\perp j_z + \nabla_\perp^2 \zeta, \tag{1}$$

$$D_t^\perp w + \partial_Z \psi = \frac{\widetilde{Ra}}{Pr} \vartheta + \widetilde{Q}\, \overline{\mathbf{B}} \cdot \nabla_\perp b_z + \nabla_\perp^2 w, \tag{2}$$

$$D_t^\perp \vartheta + w \partial_Z \overline{\Theta} = \frac{1}{Pr} \nabla_\perp^2 \vartheta, \tag{3}$$

$$\partial_Z \overline{(w\vartheta)} = \frac{1}{Pr} \partial_Z^2 \overline{\Theta}, \tag{4}$$

$$0 = \overline{\mathbf{B}} \cdot \nabla_\perp \zeta + \nabla_\perp^2 j_z, \tag{5}$$

$$0 = \overline{\mathbf{B}} \cdot \nabla_\perp w + \nabla_\perp^2 b_z. \tag{6}$$

The overbar denotes an average over fast spatiotemporal scales, and we use the notation $D_t^\perp = \partial_t + \mathbf{u}_\perp \cdot \nabla_\perp$ and $\nabla_\perp = (\partial_x, \partial_y)$. The geostrophic streamfunction (pressure) is denoted by ψ and defined by $\mathbf{u}_\perp = -\nabla_\perp \times (\psi \mathbf{e}_z)$; $\zeta = \nabla_\perp^2 \psi$ is the axial vorticity and w is the vertical velocity; ϑ and $\overline{\Theta}$ are the fluctuating and horizontally averaged temperature; $\overline{\mathbf{B}}$, b_z and $j_z = \mathbf{e}_z \cdot \nabla_\perp \times \mathbf{b}$ are the mean magnetic field, fluctuating vertical magnetic field and vertical current density, respectively; $\widetilde{Ra}$ and $\widetilde{Q}$ are, respectively, the asymptotically reduced Rayleigh and Chandrasekhar numbers (see below). For the above set of equations, time has been scaled by the small-scale (horizontal) viscous diffusion timescale l^2/ν, the magnetic field has been scaled by the magnitude of the mean magnetic field $\mathcal{B}$, and temperature has been scaled by $\Delta\theta$. We impose a mean, horizontal magnetic field defined by

$$\overline{\mathbf{B}} = \frac{\sqrt{2}}{2} \left[(\cos(\pi Z) - \cos(3\pi Z))\, \mathbf{e}_x - \cos(\pi Z) \mathbf{e}_y \right], \tag{7}$$

that satisfies perfectly conducting electromagnetic boundary conditions. Mean magnetic fields of similar spatial structure are found to be generated by dynamo action near the onset

of rotating Rayleigh-Bénard convection [12, 14, 16, 26]. Even for strongly forced convection, the mean field appears to retain a spiralling structure [12, 16]. The use of an imposed, rather than self-generated, magnetic field allows for precise control of the field magnitude. We also utilize the quasi-static MHD approximation on the small convective scale, valid for the small values of Pm typical of planetary and stellar interiors. The dynamics are controlled by three non-dimensional parameters: the asymptotically-scaled Chandrasekhar number, $\widetilde{Q} = Q_H E_H^{2/3}$ (where $Q_H = \mathcal{B}^2 H^2/(\mu_0 \rho \nu \eta)$ and μ_0 is the magnetic permeability of free space); the asymptotically-scaled Rayleigh number, $\widetilde{Ra} = Ra_H E_H^{4/3}$; and the thermal Prandtl number, $Pr = \nu/\kappa$. Here $(\widetilde{Ra}, \widetilde{Q}) = O(1)$ (or, more specifically, $\widetilde{Ra}, \widetilde{Q} < \epsilon^{-1/2}$ so that buoyancy and the Lorentz force do not enter lower orders of the asymptotic expansion) and we use $Pr = 1$ in order to allow for comparison with previous studies. For the Earth's outer core, $E_H = O(10^{-15})$, and the asymptotic model captures dynamically relevant values of $Ra_H = O(10^{20})$ and $Q_H = O(10^{10})$. The boundary conditions for (1)-(6) are impenetrable, stress-free, fixed-temperature and perfectly electrically conducting. The equations are discretized in the horizontal and vertical dimensions with Fourier series and Chebyshev polynomials, respectively. The horizontal size of the domain of integration is set to 10 times the critical wavelength at the onset of convection in both the x and y directions. The time-stepping is performed with a third order Runge-Kutta scheme [27]. Simulations of the hydrodynamical version ($\widetilde{Q} = 0$) of (1)-(6) have shown excellent quantitative agreement with laboratory experiments and DNS [17, 28].

Numerical simulations were performed over a broad range of $\widetilde{Q}$ and $\widetilde{Ra}$ (see Supplemental Material at [URL will be inserted by the publisher] for details of the numerical simulations performed in this study), allowing for the investigation of flow regimes ranging from laminar magnetoconvection, up through rapidly rotating magnetoconvective turbulence. For $\widetilde{Q} = 0$, $\widetilde{Ra} \geq 40$ generates sufficiently turbulent flows that result in the formation of an LSV [5]. The left panel of Figure 1 show instantaneous snapshots of the volume-rendered geostrophic streamfunction (pressure) and vertically integrated axial vorticity for $\widetilde{Q} = 0, \widetilde{Ra} = 160$. In the rapidly rotating limit considered here, the LSV is dipolar in structure and fills the horizontal extent of the domain such that the (energetically) dominant horizontal wavenumber is the box scale, $k = 1$, where k is the modulus of the horizontal wavenumber $\mathbf{k}$. In agreement with previous studies [5, 6, 29], the baroclinic, convective dynamics is not significantly affected by the presence of the LSV. The central and right panels of Figure 1 show the

corresponding cases with non-dimensional magnetic field strengths of $\widetilde{Q} = 1$ and $\widetilde{Q} = 2$, respectively, for $\widetilde{Ra} = 160$. It is evident that stronger magnetic fields yield a significant reduction in the strength of the horizontal box-scale mode of the depth-averaged motion, to the point that it is no longer visible.

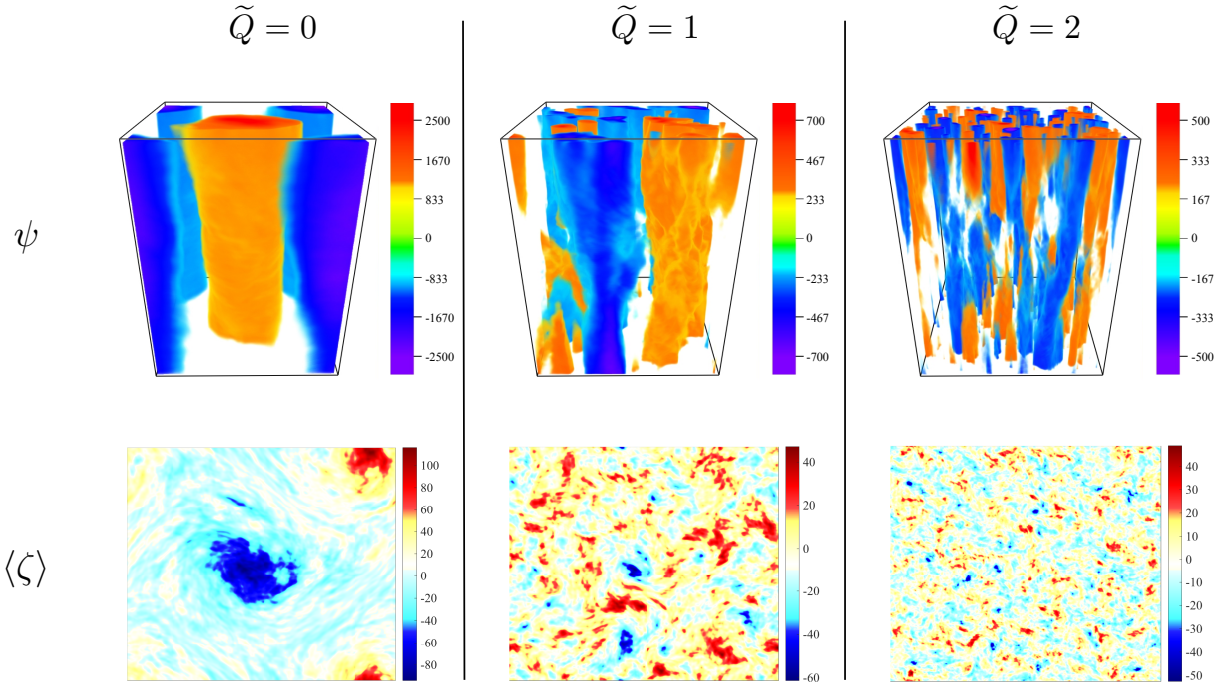

FIG. 1. Simulation snapshots. Volumetric renderings of the geostrophic streamfunction (ψ, top row) and the depth-averaged axial vorticity ($\langle\zeta\rangle$, bottom row). All plots correspond to a reduced Rayleigh number of $\widetilde{Ra} = 160$. Three values of the reduced Chandrasekhar number are shown: $\widetilde{Q} = 0$ (first column), $\widetilde{Q} = 1$ (second column) and $\widetilde{Q} = 2$ (third column).

The formation of the LSV is due to transfer of energy from the convective length-scale (where energy is injected) to the largest scales allowed in the system. This process is described by the spectral evolution equation for the barotropic (vertically integrated, horizontal) kinetic energy $K_{bt}(k)$,

$$\partial_t K_{bt}(k) = T_k + F_k + L_k + D_k. \tag{8}$$

The four terms on the right-hand side are: (1) the transfer of energy between barotropic modes of wavenumber $\mathbf{k}$,

$$T_k = \sum_{|\mathbf{k}|=k} \mathrm{Re}\left\{\langle\psi\rangle^*_{\mathbf{k}} \circ \mathcal{F}_{\mathbf{k}}\left[J[\langle\psi\rangle, \langle\zeta\rangle]\right]\right\},$$

where $\langle\psi\rangle_{\mathbf{k}}$ is the horizontal Fourier transform of the vertically averaged streamfunction $\langle\psi\rangle$, the superscript $*$ denotes a complex conjugate, $\mathcal{F}_{\mathbf{k}}[\cdot]$ indicates the horizontal Fourier transform of the argument in square brackets, $J[\cdot]$ is the Jacobian differential operator acting on the arguments in square brackets, the symbol $\circ$ indicates a Hadamard (element-wise) product (both $\langle\psi\rangle_{\mathbf{k}}$ and $\mathcal{F}_{\mathbf{k}}\left[J[\langle\psi\rangle, \langle\zeta\rangle]\right]$ are two-dimensional matrices), $\mathrm{Re}\{\cdot\}$ is the real part of the argument in curly brackets and the sum is taken over all horizontal wavenumbers; (2) the transfer of energy between the barotropic and baroclinic (convective) modes

$$F_k = \sum_{|\mathbf{k}|=k} \mathrm{Re}\left\{\langle\psi\rangle^*_{\mathbf{k}} \circ \mathcal{F}_{\mathbf{k}}\left[\langle J[\psi', \zeta']\rangle\right]\right\};$$

(3) the transfer of energy to the barotropic mode from the baroclinic magnetic field

$$L_k = -\sum_{|\mathbf{k}|=k} \widetilde{Q}\mathrm{Re}\left\{\langle\psi\rangle^*_{\mathbf{k}} \circ \mathcal{F}_{\mathbf{k}}\left[\left\langle\overline{\mathbf{B}}\cdot\nabla j'_z\right\rangle\right]\right\};$$

and (4) the viscous dissipation of the barotropic mode

$$D_k = \sum_{|\mathbf{k}|=k} \mathrm{Re}\left\{|\mathbf{k}|^2 \langle\psi\rangle^*_{\mathbf{k}} \circ \langle\zeta\rangle_{\mathbf{k}}\right\} = -2k^2 K_{bt}(k).$$

With the above definitions, positive (negative) values of T_k and F_k indicate energy is being transferred to (from) the barotropic mode k from the interaction of all the other modes. Both L_k and D_k are negative-definite.

Calculating each of the above functions allows for quantifying the transfer of energy across different spatial scales; the results are shown in Figure 2 for $\widetilde{Ra} = 160$. In the $\widetilde{Q} = 0$ case, as previously documented [5], there is a net transfer of energy to the largest scales of the barotropic mode due mostly to the non-linear interaction with the baroclinic dynamics (F_k), and partly to the interaction between different components of the barotropic flow (T_k). Since the sum of these two terms is greater than the dissipation D_k, there is a net growth of barotropic kinetic energy at large-scales, leading to the formation of the LSV. For large-scale flows, viscous friction can only become important when the flow speeds become large. Because of this, the formation of the LSV leads to a slow growth of the barotropic kinetic energy with time (see Supplemental Material at [URL will be inserted by the publisher] for time series of the kinetic energy for $\widetilde{Ra} = 40$ and $\widetilde{Ra} = 160$ cases and different values of $\widetilde{Q}$). For $\widetilde{Q} = 0.1$ the presence of the magnetic field allows for the transfer of energy between baroclinic magnetic energy and barotropic kinetic energy (via L_k), which contributes to

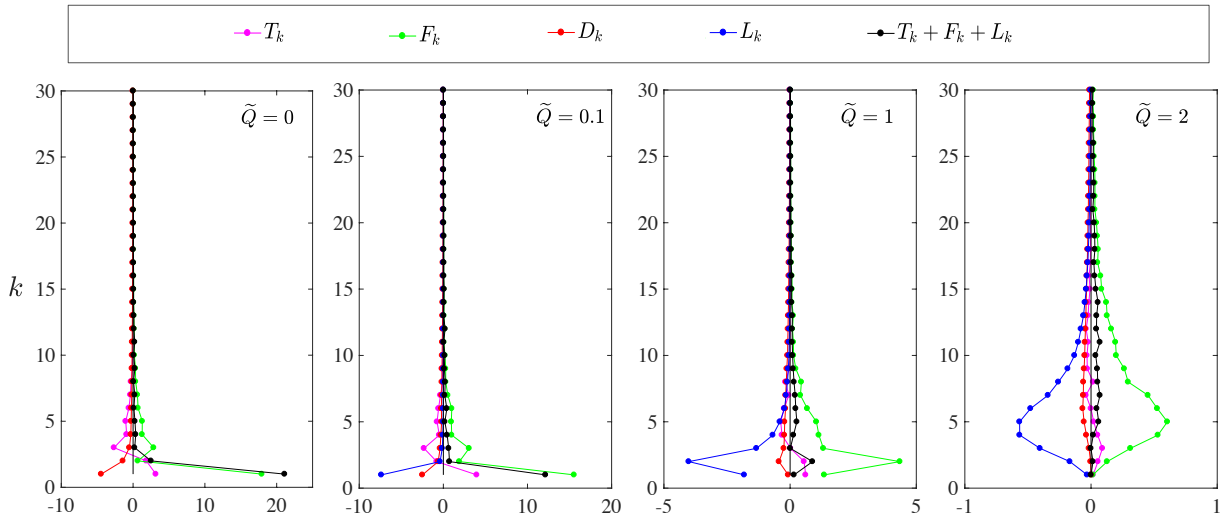

FIG. 2. Spectral energy transfer functions. All functions are averaged over a period of time in which the convective (baroclinic) dynamics are statistically stationary, as indicated by the time evolution of the vertical Reynolds number $\widetilde{Re}$ (see Supplemental Material at [URL will be inserted by the publisher] for time series of kinetic energy and $\widetilde{Re}$ for representative cases). Magnetic field strength (as characterized by the Chandrasekhar number $\widetilde{Q}$) increases from left to right, with a fixed Rayleigh number of $\widetilde{Ra} = 160$. Each plot illustrates the energetic contributions to wavenumber k of the depth-averaged (barotropic) flow, from the other baroclinic and barotropic modes (T_k and F_k), from the Lorentz force (L_k) and from viscous dissipation (D_k). Positive (negative) values indicate energy is being transferred to (from) the k-th barotropic mode.

the dissipation of energy at large-scales. Indeed, $\widetilde{Q}\left\langle \overline{\mathbf{B}}\cdot\nabla j_z'\right\rangle = -\widetilde{Q}\left\langle \sum_{\mathbf{k}} k^{-2}|\overline{\mathbf{B}}\cdot\mathbf{k}|^2\left\langle\zeta\right\rangle_{\mathbf{k}}\right\rangle$ acts as a dissipative term, proportional to the barotropic component of $\zeta_{\mathbf{k}}$. Since F_k is still dominant at larger scales, there is a net growth of barotropic kinetic energy and LSV formation. The net positive transfer of energy in these cases is due to the temporal averages being calculated over a time-span over which the inverse cascade has not been completely saturated. With time, the dissipation (both viscous and ohmic) grows in magnitude and eventually balances the baroclinic-to-barotropic and the barotropic-to-barotropic transfers, but the dominant wavenumber remains $k = 1$. As $\widetilde{Q}$ is increased we find that an inverse cascade (towards scales larger than the injection scale $k = 10$) is still present. However, F_k and T_k no longer transport energy to the largest scales (notice the kinetic energy peak at $k = 5$ for $\widetilde{Q} = 2$ in Figure 2), and the ohmic dissipation (L_k) increases in magnitude to

counterbalance F_k and T_k. LSVs do not form in such cases, leading to a rapid saturation of the kinetic energy.

In Figure 3 we show the barotropic kinetic energy spectra for the $\widetilde{Ra} = 160$ case. The formation of an LSV for $\widetilde{Q} = 0$ and $\widetilde{Q} = 0.1$ is evident by the dominance of the box-scale mode. For $\widetilde{Q} = 1$ and $\widetilde{Q} = 2$ the inverse cascade causes local maxima to be present at $k = 2$ and $k = 5$, respectively. The k^{-3} slope shown in the plot is expected in the inertial subrange, which is consistent with forward enstrophy cascade [30], and at the largest scale in presence of large-scale condensates [3, 5]. The $k = -5/3$ line is added for reference.

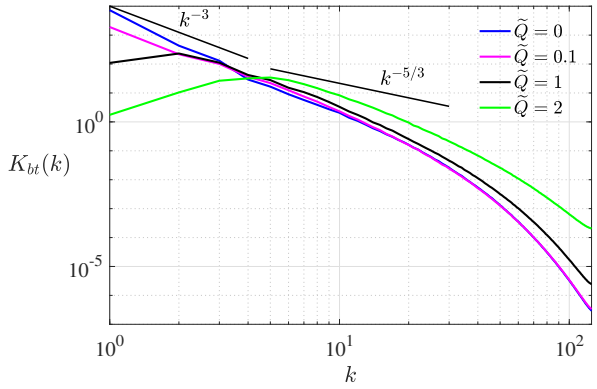

FIG. 3. Depth- and time-averaged, barotropic kinetic energy (K_{bt}) spectra for a fixed Rayleigh number of $\widetilde{Ra} = 160$ and different values of the Chandrasekhar number $\widetilde{Q}$. Lines of slope $k^{-5/3}$ and k^{-3} are shown for reference. In all cases, energy is injected through convection around $k = 10$.

For the values of $\widetilde{Ra}$ and $\widetilde{Q}$ considered here, Figure 4(a) shows that the presence of magnetic field does not have an appreciable influence on the convective (vertical) flow speeds, as characterized by the rms small-scale Reynolds number, $\widetilde{Re}$. For $\widetilde{Ra} = 160$ the relative difference in $\widetilde{Re}$ is less than 30% between the $\widetilde{Q} = 0$ and $\widetilde{Q} = 2$ cases. The threshold for LSV formation for $\widetilde{Q} = 0$ is $\widetilde{Re} \gtrsim 10$; all of the magnetic cases with $\widetilde{Ra} \gtrsim 40$ satisfy this hydrodynamic criteria, showing that $\widetilde{Re}$ alone is insufficient for determining when an LSV forms. To better characterize the conditions that favor LSV formation in the presence of magnetic field, we calculate the reduced magnetic interaction parameter $\widetilde{N}$ [31]

$$\widetilde{N} = \frac{\widetilde{Q}}{\widetilde{Re}} \simeq \frac{|\widetilde{Q}\,\overline{\mathbf{B}} \cdot \nabla_\perp \mathbf{b}|}{|\mathbf{u}_\perp \cdot \nabla_\perp \mathbf{u}_\perp|}, \tag{9}$$

where $\mathbf{b}$ and $\mathbf{u}$ are the small-scale magnetic and velocity fields, respectively. The interaction parameter is a measure of the relative magnitudes of the Lorentz force and non-linear ad-

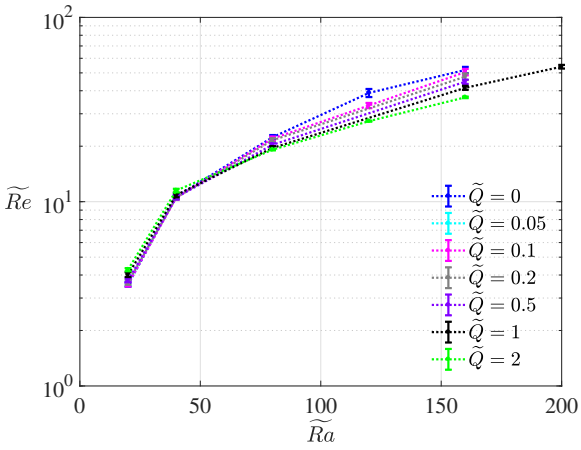

(a)

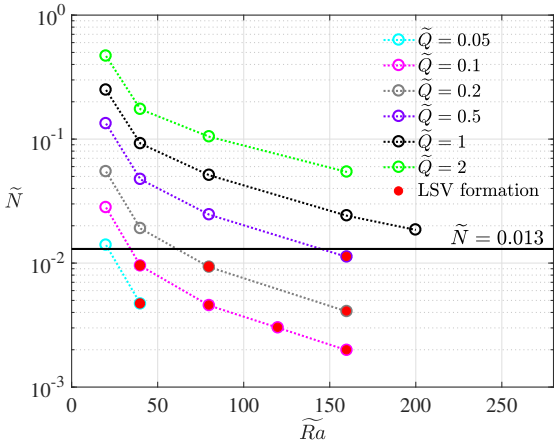

(b)

FIG. 4. (a) Reynolds number $\widetilde{Re}$ and (b) interaction parameter $\widetilde{N} = \widetilde{Q}/\widetilde{Re}$ as a function of $\widetilde{Ra}$ for different values of $\widetilde{Q}$. Values of $\widetilde{Re}$ are time averaged as in Figures 2 and 3 and the error bars in (a) represent the fluctuations around the mean value, measured by the standard deviation. Error bars on $\widetilde{N}$ would not be clearly visible on this plot and have been omitted. The filled red circles in (b) indicate large-scale vortex (LSV) formation. The black horizontal line marks the threshold $\widetilde{N} = 0.013$ above which no LSV is observed.

vection. Figure 4(b) shows that the formation of an LSV is possible for $\widetilde{N} \lesssim 0.013$. Above this threshold the magnetic field plays a significant role in the dynamics, despite the large $\widetilde{Re}$. The exact threshold value likely depends on the geometry of the mean-field.

Our results suggest that it is possible to determine whether LSVs form in natural settings, based on properties that are either directly observable, or inferred from measurements, lab-

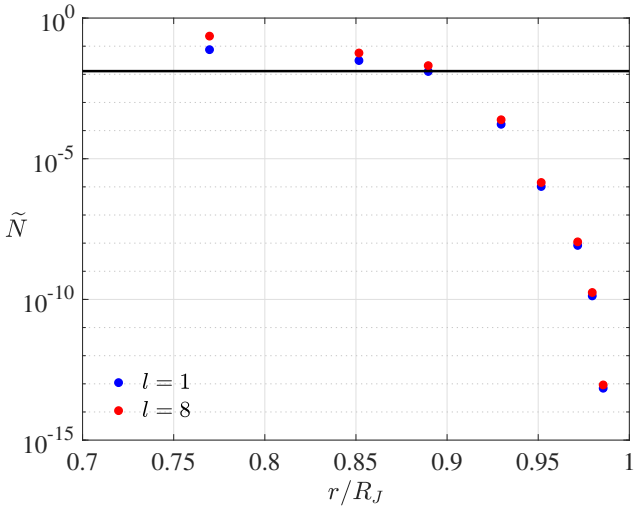

FIG. 5. Interaction parameter $\widetilde{N} = \widetilde{Re}^{-1}\widetilde{Q}$ for Jupiter as a function of the non-dimensional radius r/R_J, where R_J is the equatorial radius. The blue and red dots are calculated by estimating the large-scale magnetic field intensity to be given by the JRM09 magnetic field model [32] truncated at spherical harmonic degrees $l = 1$ and $l = 8$, respectively. The case $l = 1$ corresponds to a dipolar field and for $l > 8$ the power in the field components drops below 1% of the power contained in the dipolar field. Viscosity, electrical conductivity and density are taken from Ref. 33, and $\widetilde{Re}$ is calculated from zonally-averaged meridional flow speeds that are estimated from Cassini spacecraft observations [34]. The horizontal black line demarcates the $\widetilde{N} = 0.013$ threshold.

oratory experiments and numerical simulations. For instance, ab-initio calculations can be used to constrain the radial variation of density, viscosity and electrical conductivity within Jupiter [33]. Magnetic field models of Jupiter, as obtained from the recent Juno spacecraft observations [32], help to estimate $\widetilde{Q}$ in the outermost layers of the planet, where electrical conductivity is small. To estimate $\widetilde{Re}$ we use zonal-mean meridional velocities derived from Cassini spacecraft observations [34], which most likely constitute a lower bound on the convective velocities, and assume they do not change significantly with depth. Together, this data suggests that $\widetilde{N} \geq 0.013$ for $r \lesssim 0.87R_J$, where r is the distance from the center of Jupiter and R_J is the equatorial radius (see Figure 5). This depth agrees with the location of the dynamo region's upper limit estimated from ab-initio calculations [33], from numerical simulation results [35] and from the depth of zonal flows based on Juno's gravitational field observations [36] (although it is somewhat deeper than the estimated depth reached

by deep zonal jets [36–38]), suggesting that the observed large-scale vortices [39] and winds do not penetrate into the dynamo region of Jupiter. For the Earth's outer core we estimate $\widetilde{Re} = 10^3$ and $\widetilde{Q} \approx 3 \times 10^5$ for accepted values of core flow speed and viscosity [40] and a magnetic field intensity of 3 mT [41]. These two values give $\widetilde{N} \approx 300$, which is well above the threshold of $\widetilde{N} \approx 0.013$ identified from Figure 4(b). We conclude that, at the present time, convectively-generated LSVs are likely not present in the Earth's core.

ACKNOWLEDGEMENTS

This work was supported by the National Science Foundation under grant EAR #1620649 (SM, MAC and KJ). This work utilized the RMACC Summit supercomputer, which is supported by the National Science Foundation (awards ACI-1532235 and ACI-1532236), the University of Colorado Boulder, and Colorado State University. The Summit supercomputer is a joint effort of the University of Colorado Boulder and Colorado State University. Volumetric rendering was performed with the visualization software VAPOR.

---

[1] P Olson, "Core dynamics: an introduction and overview," Treatise on Geophysics , 1–25 (2015).

[2] N. Schaeffer, D. Jault, H.-C. Nataf, and A. Fournier, "Turbulent geodynamo simulations: a leap towards Earth's core," Geophysical Journal International **211**, 1–29 (2017).

[3] Leslie M Smith and Fabian Waleffe, "Transfer of energy to two-dimensional large scales in forced, rotating three-dimensional turbulence," Physics of fluids **11**, 1608–1622 (1999).

[4] Benjamin Favier, L J Silvers, and M R E Proctor, "Inverse cascade and symmetry breaking in rapidly rotating Boussinesq convection," Physics of Fluids **26**, 096605 (2014).

[5] Antonio M Rubio, Keith Julien, Edgar Knobloch, and Jeffrey B Weiss, "Upscale energy transfer in three-dimensional rapidly rotating turbulent convection," Physical Review Letters **112**, 144501 (2014).

[6] Céline Guervilly, David W Hughes, and Chris A Jones, "Large-scale vortices in rapidly rotating Rayleigh–Bénard convection," Journal of Fluid Mechanics **758**, 407–435 (2014).

[7] Thomas Le Reun, Benjamin Favier, Adrian J Barker, and Michael Le Bars, "Inertial wave turbulence driven by elliptical instability," Physical Review Letters **119**, 034502 (2017).

[8] Céline Guervilly, David W Hughes, and Chris A Jones, "Generation of magnetic fields by large-scale vortices in rotating convection," Physical Review E **91**, 041001 (2015).

[9] Peter B Rhines, "Waves and turbulence on a beta-plane," Journal of Fluid Mechanics **69**, 417–443 (1975).

[10] Simon Cabanes, Jonathan Aurnou, Benjamin Favier, and Michael Le Bars, "A laboratory model for deep-seated jets on the gas giants," Nature Physics **13**, 387 (2017).

[11] Yufeng Lin, Philippe Marti, Jerome Noir, and Andrew Jackson, "Precession-driven dynamos in a full sphere and the role of large scale cyclonic vortices," Physics of Fluids **28**, 066601 (2016).

[12] Céline Guervilly, David W Hughes, and Chris A Jones, "Large-scale-vortex dynamos in planar rotating convection," Journal of Fluid Mechanics **815**, 333–360 (2017).

[13] Michael A. Calkins, Keith Julien, Steven M. Tobias, and Jonathan M. Aurnou, "A multiscale dynamo model driven by quasi-geostrophic convection," Journal of Fluid Mechanics **780**, 143–166 (2015).

[14] A. M. Soward, "A convection-driven dynamo: I. the weak field case," Philosophical Transactions of the Royal Society A **275**, 611–646 (1974).

[15] M. A. Calkins, K. Julien, S. M. Tobias, J. M. Aurnou, and P. Marti, "Convection-driven kinematic dynamos at low Rossby and magnetic Prandtl numbers: single mode solutions," Phys. Rev. E. **93**, 023115 (2016).

[16] M. A. Calkins, L. Long, D. Nieves, K. Julien, and S. M. Tobias, "Convection-driven kinematic dynamos at low Rossby and magnetic Prandtl numbers," Physical Review Fluids **1**, 083701 (2016).

[17] S Stellmach, M Lischper, K Julien, G Vasil, J S Cheng, A Ribeiro, E M King, and J M Aurnou, "Approaching the asymptotic regime of rapidly rotating convection: boundary layers versus interior dynamics," Physical Review Letters **113**, 254501 (2014).

[18] Murshed Hossain, "Inverse energy cascades in three-dimensional turbulence," Physics of Fluids B: Plasma Physics **3**, 511–514 (1991).

[19] Alexandros Alexakis, "Two-dimensional behavior of three-dimensional magnetohydrodynamic flow with a strong guiding field," Physical Review E **84**, 056330 (2011).

[20] K Sandeep Reddy and Mahendra K Verma, "Strong anisotropy in quasi-static magnetohydrodynamic turbulence for high interaction parameters," Physics of Fluids **26**, 025109 (2014).

[21] Steven M Tobias, Patrick H Diamond, and David W Hughes, "β-plane magnetohydrodynamic turbulence in the solar tachocline," The Astrophysical Journal Letters **667**, L113 (2007).

[22] Kannabiran Seshasayanan, Santiago Jose Benavides, and Alexandros Alexakis, "On the edge of an inverse cascade," Physical Review E **90**, 051003 (2014).

[23] Michael Sprague, Keith Julien, Edgar Knobloch, and Joseph Werne, "Numerical simulation of an asymptotically reduced system for rotationally constrained convection," Journal of Fluid Mechanics **551**, 141–174 (2006).

[24] Meredith Plumley, Michael A Calkins, Keith Julien, and Steven M Tobias, "Self-consistent single mode investigations of the quasi-geostrophic convection-driven dynamo model," Journal of Plasma Physics **84** (2018).

[25] Subrahmanyan Chandrasekhar, *Hydrodynamic and Hydromagnetic stability* (Courier Corporation, 1961).

[26] Stephan Stellmach and Ulrich Hansen, "Cartesian convection driven dynamos at low Ekman number," Physical Review E **70**, 056312 (2004).

[27] Philippe R Spalart, Robert D Moser, and Michael M Rogers, "Spectral methods for the navier-stokes equations with one infinite and two periodic directions," Journal of Computational Physics **96**, 297–324 (1991).

[28] Meredith Plumley, Keith Julien, Philippe Marti, and Stephan Stellmach, "The effects of Ekman pumping on quasi-geostrophic Rayleigh–Bénard convection," Journal of Fluid Mechanics **803**, 51–71 (2016).

[29] K Julien, A M Rubio, I Grooms, and E Knobloch, "Statistical and physical balances in low Rossby number Rayleigh–Bénard convection," Geophysical & Astrophysical Fluid Dynamics **106**, 392–428 (2012).

[30] Robert H Kraichnan, "Inertial ranges in two-dimensional turbulence," The Physics of Fluids **10**, 1417–1423 (1967).

[31] S Cioni, S Chaumat, and J Sommeria, "Effect of a vertical magnetic field on turbulent Rayleigh-Bénard convection," Physical Review E **62**, R4520 (2000).

[32] J E P Connerney, S Kotsiaros, R J Oliversen, J R Espley, John Leif Joergensen, P S Joergensen, José M G Merayo, Matija Herceg, J Bloxham, K M Moore, *et al.*, "A new model

of Jupiter's magnetic field from Juno's first nine orbits," Geophysical Research Letters **45**, 2590–2596 (2018).

[33] Martin French, Andreas Becker, Winfried Lorenzen, Nadine Nettelmann, Mandy Bethkenhagen, Johannes Wicht, and Ronald Redmer, "Ab initio simulations for material properties along the Jupiter adiabat," The Astrophysical Journal Supplement Series **202**, 5 (2012).

[34] Boris Galperin, Roland MB Young, Semion Sukoriansky, Nadejda Dikovskaya, Peter L Read, Andrew J Lancaster, and David Armstrong, "Cassini observations reveal a regime of zonostrophic macroturbulence on Jupiter," Icarus **229**, 295–320 (2014).

[35] Lúcia DV Duarte, Thomas Gastine, and Johannes Wicht, "Anelastic dynamo models with variable electrical conductivity: An application to gas giants," Physics of the Earth and Planetary Interiors **222**, 22–34 (2013).

[36] Dali Kong, Keke Zhang, Gerald Schubert, and John D Anderson, "Origin of Jupiter's cloud-level zonal winds remains a puzzle even after Juno," Proceedings of the National Academy of Sciences **115**, 8499–8504 (2018).

[37] Y Kaspi, E Galanti, W B Hubbard, D J Stevenson, S J Bolton, L Iess, T Guillot, J Bloxham, J E P Connerney, H Cao, *et al.*, "Jupiter's atmospheric jet streams extend thousands of kilometres deep," Nature **555**, 223 (2018).

[38] Tristan Guillot, Y Miguel, B Militzer, W B Hubbard, Y Kaspi, E Galanti, H Cao, R Helled, S M Wahl, L Iess, *et al.*, "A suppression of differential rotation in Jupiter's deep interior," Nature **555**, 227 (2018).

[39] Alberto Adriani, A Mura, G Orton, C Hansen, F Altieri, M. L. Moriconi, J Rogers, G Eichstädt, T Momary, A P Ingersoll, *et al.*, "Clusters of cyclones encircling Jupiter's poles," Nature **555**, 216 (2018).

[40] Chris A Jones, "Thermal and compositional convection in the outer core," Treatise on Geophysics , 115–159 (2015).

[41] Nicolas Gillet, Dominique Jault, Elisabeth Canet, and Alexandre Fournier, "Fast torsional waves and strong magnetic field within the Earth's core," Nature **465**, 74–77 (2010).